ACS central science

Research Article

Cite This: ACS Cent. Sci. 2018, 4, 820−831

Hydrophobic Hydration and the Effect of NaCl Salt in the Adsorption of Hydrocarbons and Surfactants on Clathrate Hydrates

Felipe Jiménez-Ángeles[†] and Abbas Firoozabadi*[,†,‡]

[†]Reservoir Engineering Research Institute, Palo Alto, California 94301, United States

[‡]Department of Chemical and Environmental Engineering, Yale University, New Haven, Connecticut 06510, United States

Supporting Information

ABSTRACT: Adsorption of functional molecules on the surface of hydrates is key in the understanding of hydrate inhibitors. We investigate the adsorption of a hydrocarbon chain, nonionic and ionic surfactants, and ions at the hydrate−aqueous interface. Our results suggest a strong connection between the water ordering around solutes in bulk and the affinity for the hydrates surface. We distinguish two types of water ordering around solutes: (i) hydrophobic hydration where water molecules form a hydrogen bond network similar to clathrate hydrates, and (ii) ionic hydration where water molecules align according to the polarity of an ionic group. The nonionic surfactant and the hydrocarbon chain induce hydrophobic hydration and are favorably adsorbed on the hydrate surface. Adsorption of ions and the ionic headgroups on the hydrate surface is not favorable because ionic hydration and the hydrogen bond structure of hydrates are incompatible. The nonionic surfactant is adsorbed by the headgroup and tail while adsorption of the ionic surfactants is not favorable through the head. Water ordering is analyzed using the hydrogen bond and tetrahedral density profiles as a function of the distance to the chemical groups. The adsorption of solutes is studied through the free energy profiles as a function of the distance to the hydrate surface. Salt lowers the melting temperature of hydrates, disrupts hydrophobic hydration, reduces the solubility of solutes in the aqueous solution, and increases the propensity of solutes to be adsorbed on hydrate surfaces. Our studies are performed by the unbiased and steered molecular dynamics simulations. The results are in line with experiments on the effect of salt and alkanes in hydrate antiagglomeration.

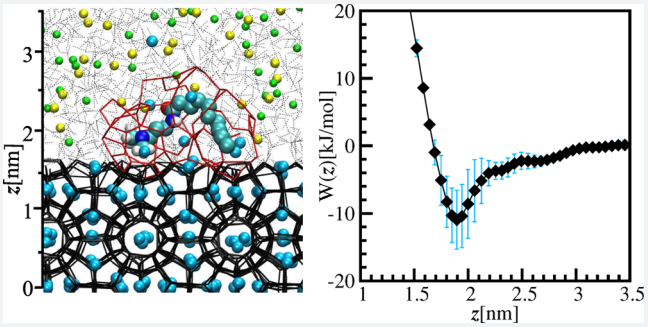

INTRODUCTION

Clathrate hydrates are crystalline structures of hydrogen-bonded water molecules where guest molecules, such as methane, propane, carbon dioxide, and nitrogen, are encaged. Ions are not found as guests in hydrates. The cages in hydrates are designated as $4^l5^m6^n$, where l, m, and n represent the number of square, pentagonal, and hexagonal faces. The lattice structure of clathrate hydrates is defined by the geometry and the number of cages in the unit cell. The unit cell of structure I (sI) is formed by two 6^{12} and six $5^{12}6^2$ cages; the unit cell of structure II (sII) is formed by 16 5^{12} cages and eight $5^{12}6^4$ cages, and the unit cell of structure H (sH) is formed by two 5^{12} cages, two $4^35^66^3$ cages, and one $5^{12}6^8$ cage.[1,2]

Natural gas hydrates are important in energy production both as a methane resource stored in hydrates at the ocean floor, and as a safety and environmental concern during hydrocarbon production. Hydrates may form swiftly during hydrocarbon transport and obstruct the flowlines. Knowledge of nucleation and growth is essential for the exploitation and utilization of hydrates. A number of molecular simulation studies have been conducted to reveal the early stages of hydrates nucleation of clathrate hydrates.[3−14] The use of surfactants in the hydrate research fields is of broad interest in flow-assurance and gas storage.[15−23]

In the energy industry hydrate mitigation is often by means of chemical additives. Hydrate inhibitors are classified as thermodynamic inhibitors (TIs) and low dosage inhibitors (LDIs).[24,25] Thermodynamic inhibitors (such as methanol and glycol) and ions[26,27] shift the hydrate formation conditions to lower temperature and higher pressure. Low dosage hydrate inhibitors are classified as kinetic inhibitors and agglomeration inhibitors.[28] Hydrate kinetic inhibitors (HKIs) delay the onset of nucleation or slow the hydrates growth rate. Common HKIs are soluble polymers of amide groups such as *N*-vinyl-pirrolidone, *N*-vinylcaprolactam, and *N*-vinylacetamide.[29] Amphiphilic molecules[1,25,28,30,31] are used as hydrate agglomeration inhibitors (HAIs) which prevent the coalescence of small hydrate crystallites to ensure fluid flow as a slurry. The nucleation rate of clathrate hydrates, however, may increase in the presence of some anionic surfactants such as sodium dodecyl sulfate.[15−20] Antifreeze proteins are suggested as a green alternative of gas hydrate inhibition.[32−36]

Received: February 1, 2018
Published: June 21, 2018

DOI: 10.1021/acscentsci.8b00076
ACS Cent. Sci. 2018, 4, 820−831

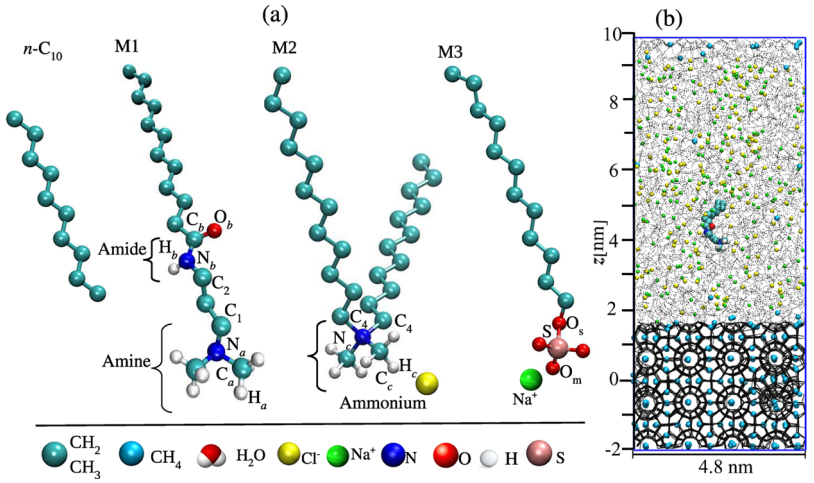

Figure 1. (a) Molecular structure of the solute molecules: *n*-decane (n-C_{10}); molecule M1, cocamidopropyl dimethylamine; molecule M2, didodecyl dimethylammonium chloride; molecule M3, sodium dodecyl sulfate. Indexes *a*, *b*, and *c* designate atoms in the amine, amide, and ammonium groups, respectively. The partial charges are provided in Tables S1−S3 in the SI. (b) Snapshot of the simulation setup containing a hydrate slab next to an aqueous solution containing one surfactant molecule M1. The crystal slab is made of 2208 water molecules and 384 methane molecules; the aqueous phase contains one solute molecule (n-C_{10}, M1, M2, or M3), 5700 water molecules, and N_s NaCl ionic pairs; N_s = 0, 72, and 180 at 0, 4, and 10 NaCl wt %, respectively. The hydrogen bonds in the hydrate slab are represented as black sticks and as thin black lines in the aqueous phase. The color key for various species is at the bottom.

Understanding the adsorption of surfactants on hydrate surfaces is essential in flow-assurance and gas storage. To a great extent, the efficiency of low dosage hydrate inhibitors (kinetic and antiagglomerants) is determined by the adsorption on the hydrates surface.[25,28,29,37,38] Hydrogen bonding[39,40] and structural fit[37] are suggested as the origin of binding between the hydrate surface and the inhibitors. Molecular simulations are employed to shed light into the adsorption mechanisms of hydrate inhibitors.[29,39−47] According to Anderson et al.[29] two molecular characteristics lead to a strong binding of inhibitors on the hydrate surface: a charge distribution on the edge of the inhibitor similar to water molecules and the size congruence between the inhibitor group and the open cavities at the hydrate surface. Yagasaki et al.[45] found no hydrogen bonding between the kinetic inhibitor vinylpirrolidone and the hydrate surface in opposition to the conventional picture. According to recent MD simulations, the adsorption of a quaternary ammonium surfactant at the surface of sII hydrates is stronger from a liquid hydrocarbon phase than from an aqueous phase.[48]

The water structure around hydrophobic and amphiphilic molecules (known as hydrophobic hydration) has some similarities with the structure of hydrates and has been observed in different studies.[49−56] The idea of hydrophobic hydration can be traced back to a thermodynamic model of dissolution where it is proposed that water molecules form transient clathrate-like clusters around hydrophobic molecules.[57] Recent spectroscopic experiments confirm the picture of hydrophobic hydration by measuring hydrogen bond enhancement of water near hydrophobic solutes.[56] It is suggested that hydrophobic hydration plays a fundamental role in hydrophobic forces.[58−60] Here we will show that hydrophobic hydration around solutes is related to the affinity of chemical groups for the surface of hydrates.

Recently we have performed an experimental investigation of salt and alkane hydrocarbon concentration on hydrate antiagglomeration.[61,62] The surfactant molecule M1 which will be described later was used an antiagglomerant. Salt enhances hydrate antiagglomerations. Normal alkanes (normal decane) also enhance hydrate antiagglomeration. In the hydrate literature the effect of hydrocarbons is often expressed in terms of the ratio of water to hydrocarbon liquids as water cut. It is well-known that at high water cuts hydrate antiagglomeration is facilitated. There has been no theoretical explanation for the effect of hydrocarbons except some general bulk solubility effects. The interaction of ionic and nonionic surfactants with hydrates is not understood. The main objective of this work is to examine the mechanism of adsorption of solute molecules at the hydrate−aqueous interface and the effect of NaCl in the process. The solutes are *n*-decane, a nonionic surfactant (cocamidopropyl dimethylamine), a cationic surfactant (didodecyl dimethylammonium chloride), and an anionic surfactant (sodium dodecyl sulfate). First, we analyze the structure of water molecules around solutes in an aqueous phase; the structure of water around methane is also investigated. Next, we study the adsorption of solute molecules at the hydrate−aqueous phase interface. The effect of NaCl is investigated at the concentrations of 0, 4, and 10 NaCl wt %. A key objective of this work is a molecular explanation of the salt effect and normal alkane effect on hydrate antiagglomeration. The remainder of the paper is organized as follows: simulation models and methods; the results split in two subsections, solutes in the bulk and adsorption of solutes on methane hydrate surface; discussion and conclusions drawn at the end of the paper. The SI contains a discussion of the effect of salt in hydrate three-phase equilibrium, additional results and details of the calculation methods, verification of the steered molecular dynamics technique, and tables.

Figure 1 shows *n*-decane and the surfactants investigated in this work. Molecule M1 has been used as an effective antiagglomerant.[31,63,64] Molecule M2 is an ionic quaternary ammonium surfactant (QAS) which is effective in hydrate antiagglomeration where there is a significant amount of liquid hydrocarbons.[64] Molecule M3 is sodium dodecyl sulfate (SDS) which is known to increase the nucleation rate of clathrate hydrates.[15−18]

DOI: 10.1021/acscentsci.8b00076
ACS Cent. Sci. 2018, 4, 820−831

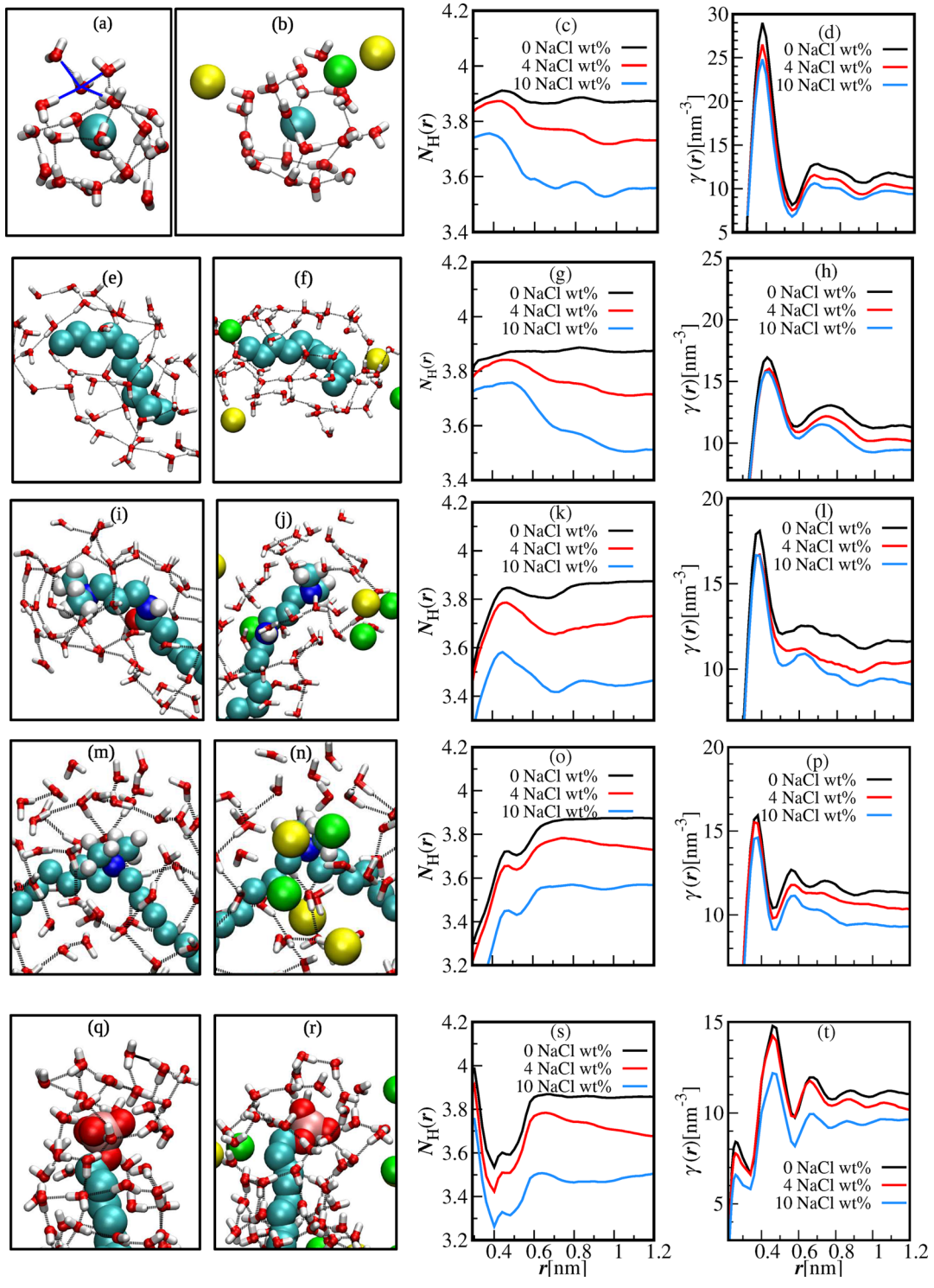

Figure 2. Structure of water molecules around the solute molecules. Each row contains two instantaneous snapshots showing the water molecules at a distance of $r < 0.52$ nm from the solute molecules at 0 and 10 NaCl wt %; the number of hydrogen bonds per water molecule $N_H(r)$ and the density of tetrahedral water $\gamma(r)$ at a distance r from a selected site. (a–d) Methane, (e–h) *n*-decane, and $N_H(r)$ and $\gamma(r)$ are from the fifth carbon atom; (i–l) molecule M1 and $N_H(r)$ and $\gamma(r)$ are from the CH_3 methyl head groups; (m–p) molecule M2 and $N_H(r)$ and $\gamma(r)$ are from the CH_3 methyl head groups; (q–t) molecule M3 and $N_H(r)$ and $\gamma(r)$ are from the oxygen atoms of the SDS headgroup. The dashed lines in the snapshots represent the hydrogen bonds; the solid blue line in part a highlights a tetrahedral structure; T = 277 K, and P = 300 bar.

RESULTS

Solutes in the Bulk. We analyze the water structure around hydrocarbon molecules, methane, and *n*-C_{10} and surfactant molecules at different salt concentrations. The structural changes of water around methane are not captured in the radial distribution function (see Figure S5 in the SI); only slight changes are observed by increasing the salt concentration[65,66] from 0 to 10 NaCl wt %. The changes occur in the hydrogen bond and tetrahedral structure of water molecules surrounding the solute. Water molecules form

DOI: 10.1021/acscentsci.8b00076
ACS Cent. Sci. 2018, 4, 820–831

instantaneous hydrate-like structures around methane, namely, pentagonal and hexagonal rings (Figure 2a). At 10 NaCl wt % the ions disrupt some of the hydrogen bonds around the methane molecule (see Figure 2b).

Hydrophobic solutes induce temporary hydrogen bond structures resembling those in hydrates known as hydrophobic hydration. Ionic groups tend to align the dipole moment of water. We study the structural changes of water by means of the hydrogen bond and tetrahedral structures. A hydrogen bond forms when the center−center distance of two water oxygen atoms is less than 0.35 nm, and the two oxygen atoms make an angle less than 25° with a hydrogen atom belonging to one of the water molecules. In the particular case of molecule M3 (SDS), we consider the oxygen headgroup atoms as hydrogen bond acceptors. We define $N_H(r)$ as the average number of hydrogen bonds per water molecule at a distance r from a site i. A water molecule in a perfect tetrahedron forms four hydrogen bonds; the angle formed between two hydrogen bonds is about 109.5°. Water molecules in tetrahedrons are found in ice and hydrates.[67] A measure of the deviation of tetrahedrality is given by the order parameter $q = \sum_{j=1}^{n_i} \sum_{k=j+1}^{n_i} (|\cos \theta_{ijk}| \cos \theta_{ijk} + {}^1/_9)^2$, where n_i is the number of nearest neighbors of water molecule i, and θ_{ijk} is the angle between the oxygen atoms of water molecules j, i, and k. A water molecule is considered tetrahedral if it has $q < 0.4$ and is coordinated with at least three water molecules. This classification was proposed by Baez and Clancy[68] and has been used in a number of studies.[12,13] We define $\gamma(r)$ as the average number density of tetrahedral water molecules at a distance r from a site i of a molecule. The averages are taken over 5×10^3 independent configurations from over 20 ns of MD simulation.

Figure 2c portrays the average number of hydrogen bonds of a water molecule at a distance r from the center of a methane molecule. At zero salt concentration the maximum number of hydrogen bonds is around 3.85 at $r \approx 0.48$ nm. Lower values of N_H are observed as the salt concentration increases. Our prediction of the number of hydrogen bonds as a function of the distance to the methane molecule is in agreement with the calculations reported by Grdadolnik et al.[56] in a recent study of the hydrogen bond strength of water near small hydrophobic solutes. The increase in both salt concentration and temperature decreases the number of hydrogen bonds. The number density of tetrahedral water γ reflects the icelike structure of water. Figure 2d shows γ as a function of the distance to a methane molecule. The density of tetrahedral water is significantly higher close to the methane molecule than in the bulk; at zero salt concentration the density of tetrahedral water is nearly 3 times higher than in the bulk. As the salt concentration increases the number of tetrahedral water molecules close to methane molecule decreases but always is at least 2 times higher than in the bulk.

Ions stay away from methane molecules[65,69] due to dielectric changes of the medium. Ions stay favorably hydrated in the liquid phase. Bringing an ion close to a methane molecule implies an energy penalty of dehydration and competition with hydrogen bond structures. The free energy of transferring methane from the gas phase into the aqueous phase ΔG is given by $\Delta G = -k_B T \ln P_{v_0}(0)$ where $P_{v_0}(0)$ is the probability of finding a cavity of volume v_0 free of solvent molecules. Our results confirm the view of dissolution of methane in water by formation of transient hydrate-like structures.[57] The water-free cavity is stabilized by the clathrate-like structures. Ions destabilize the hydrogen bond structures; hence, the probability to form a water-free cavity in the aqueous phase decreases in the presence of NaCl. In other words, the free energy of placing a methane molecule into the aqueous phase increases by increasing the salt concentration.[66]

Figure 2e,f shows instantaneous structures of water molecules around n-decane at 0 and 10 NaCl wt %, respectively. Water molecules form instantaneous pentagonal and hexagonal rings mainly at the end methyl groups of the n-decane molecule while the hydrogen bond network is disconnected in the methylene group at the middle of the molecule. Non-hydrogen-bonded water molecules form dangling OH groups which are seen as defects in water's hydrogen-bonding network.[52,53] In our MD simulations, dangling OH groups around n-decane are mainly observed at the middle of the molecule. At 10 NaCl wt %, ions disrupt the hydrate-like structure around n-decane (see Figure 2f). Figure 2g,h shows, respectively, the average number of hydrogen bonds per water molecule and the tetrahedral density from a CH_2 methylene group at the middle of the n-decane molecule. $N_H(r)$ and $\gamma(r)$ functions calculated from the CH_3 end methyl group are provided in the SI (Figure S6). The number density of tetrahedral water around the CH_3 groups is lower than around methane because the hydrocarbon chain obstructs the connectivity among the water molecules. The obstruction is pronounced at the middle of the n-decane molecule, and the number density of tetrahedral water is significantly reduced; at zero salt concentration the maximum tetrahedral density is 29, 22, and 17 molecules/nm^3 in methane, CH_3, and the middle CH_2 of n-decane, respectively. The number of hydrogen bonds per water molecules is similar to methane in both CH_2 and CH_3 groups of n-decane (see Figure S6 in the SI).

Figure 2i,j is snapshots of water molecules around molecule M1 at 0 and 10 NaCl wt %, respectively. We see instantaneous hydrate-like rings around the surfactant head and tail. The hydrate-like structures are disrupted by the ions at 10 NaCl wt % (see Figure 2j). The average number of hydrogen bonds of a water molecule at a distance r from the CH_3 groups in the head is shown in Figure 2k, and the number density of tetrahedral water is presented in Figure 2l. The number of hydrogen bonds below $r \approx 0.38$ nm is lower than in the bulk because water molecules cannot access this region. The maximum number of hydrogen bonds and the number of tetrahedral water is located at $r \approx 0.4$ nm. Our results imply that a shell of hydrate-like water is formed around the head of molecule M1. Similarly to methane and n-decane, the number of hydrogen bonds per water molecule is reduced by NaCl salt. The hydrate-like structure of water is higher around the surfactant head than in the bulk; the density of tetrahedral water is less affected by NaCl ions close to the surfactant head than in the bulk. Around the tail of molecule M1 the water molecules behave similarly as in the n-decane molecule; that is, more tetrahedral structures form around the tail end while in the middle of the tail the tetrahedral structure is reduced. We observe dangling OH groups around the amide group in the middle of molecule M1 due to the electrostatic attraction between the amide oxygen atom and the water hydrogen atoms.

Hydration around ionic groups (ionic hydration) is different from hydrophobic hydration. Usually the dipole moment of water tends to be aligned by the electrostatic interaction with ionic groups. Instantaneous arrangements of water molecules around molecule M2 are shown in Figure 2m,n at 0 and 10

DOI: 10.1021/acscentsci.8b00076
ACS Cent. Sci. 2018, 4, 820−831

NaCl wt %, respectively. Typically, the water molecules are oriented with the oxygen atom pointing toward the cationic headgroup. At zero salt concentration the hydrogen bond network is open around the surfactant head. At 10 NaCl wt % ions are close to the surfactant head, and no closed hydrogen bond network is formed. At the two tail ends the hydrate-like structure is similar to *n*-decane. The average number of hydrogen bonds of a water molecule is below the bulk value for $r \lesssim 0.6$ (Figure 2o). The number density of tetrahedral water is much lower around the head of M2 than around the head of M1 (see Figure 2l,p). The non-hydrogen-bonded water molecules form dangling OH groups pointing outward from the ionic headgroup due to the electrostatic repulsion between the hydrogen atoms and cationic ammonium group.

A water molecule close to the SDS headgroup is usually found with a hydrogen atom pointing toward the oxygen atom of SDS (see Figure 2q,r). Hence, we consider the oxygen atoms of SDS as hydrogen bond acceptors. From this consideration we find significant differences between the water structures around the headgroup of molecule M3 and the other molecules. In particular, we see a maximum of N_H at $r \approx 0.3$ nm for SDS (M3, see Figure 2s) while the other molecules have a decreasing behavior at similar distances (Figure 2o); for 0 NaCl wt % $N_H = 4$ at $r \approx 0.3$ nm which indicates perfect tetrahedral coordination of a water molecule. For M3 γ has a small peak at $r \approx 0.28$ nm (Figure 2t) which is not observed for the other molecules (Figure 2d,h,l,p). Our results indicate that the anionic surfactant headgroup induces the formation of hydrogen bonds and tetrahedral water which may be related to the increase of hydrate nucleation rate.[15−18] The water structure around the SDS headgroup is different from hydrophobic hydration. As usual, NaCl decreases the formation of hydrogen bonds and tetrahedral structures.

In Raman scattering measurements of the hydrophobic hydration shell around hydrophobic solutes,[51] it is found that chains longer than 1 nm have weaker hydrogen bonds than bulk water, and the structure is less ordered. Our MD simulation results for *n*-decane show that the hydration layer is broken, and tetrahedrality is significantly reduced at the middle of the chain. A defective hydrogen bond network with a variable number of dangling OH groups (non-hydrogen-bonded water molecules) is observed in linear alcohols and other amphiphilic solutes;[52,53] the number of dangling OHs is significantly lower for ammonium ions than for alcohols. We observe dangling OH groups in the hydrate-like network around surfactants and hydrophobic solutes. In our MD simulation results, a significant reduction of the hydrogen bond network and dangling OH groups are observed around the ammonium group in agreement with the experimental measurements.[52,53]

Adsorption of Solutes on Methane Hydrate Surface. Now we investigate the adsorption of *n*-decane, a nonionic surfactant M1, a cationic surfactant M2, and an anionic surfactant M3 on the hydrate surface. We observe the segments of the solute molecules preferentially adsorbed induce hydrate-like structures around them (hydrophobic hydration). The preferential adsorption of hydrophobic molecules is related to the effect of an oil phase in hydrate antiagglomeration. The addition of NaCl salt enhances the adsorption of the surfactants on the hydrate surface. The enhancement of surfactant adsorption from the salt effect is in line with experimental observations.[61,62] The molecular mechanisms will become clear in the following investigations.

The free energy profiles of adsorption of *n*-decane at 0, 4, and 10 NaCl wt % are shown in Figure 3a−c, respectively. The

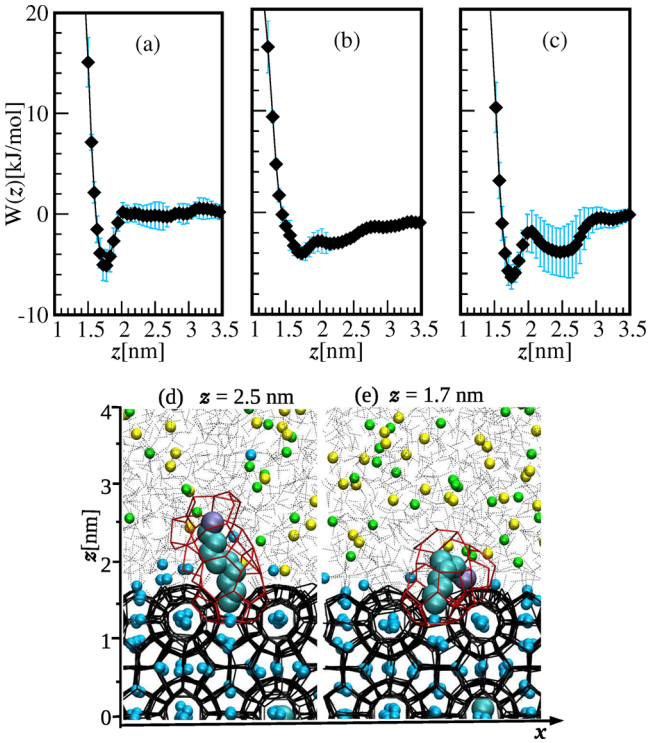

Figure 3. Adsorption of *n*-decane molecule on the surface of methane hydrate (sI). Potential of mean force $W(z)$ as a function of the distance between the steered methyl group and the hydrate slab; the origin is set inside the hydrate slab (see Figure 1b). The NaCl salt concentration is (a) 0, (b) 4, and (c) 10 NaCl wt %. Snapshots of *n*-decane molecule at 10 NaCl wt % when the pulled methyl group (ice-blue particle) is at (d) $z \approx 2.5$ nm and (e) $z \approx 1.7$ nm. The red thin lines show hydrogen bonding around *n*-decane molecule. The spring constant is $k = 2000$ kJ/(mol nm^2); the pulling velocity is 5×10^{-3} nm/ns, $P = 300$ bar, and $T = 277$ K.

error bars are computed from three independent simulations. Figure 3d shows the configuration of *n*-decane when the steered methyl group is at $z \approx 2.5$ nm, and the free methyl group is adsorbed on the hydrate surface; Figure 3e shows the steered methyl group at $z \approx 1.7$ nm adsorbed on the hydrate surface. There is a decrease of the free energy of adsorption of *n*-decane as the salt concentration increases. At 0 NaCl wt % (Figure 3a) there is a free energy drop of about −1 kJ/mol when the steered methyl group is at $z \approx 2.5$ nm, and the free methyl group is adsorbed on the hydrate surface. A minimum of about −4.5 kJ/mol depth at $z \approx 1.7$ nm is observed when the pulled methyl group is adsorbed on the hydrate surface. A steep increase of the free energy profile is observed for $z \lesssim 1.7$ nm implying that further penetration of *n*-decane into the hydrate solid structure is obstructed by the strongly hydrogen-bonded water molecules that require a high energy cost to be removed. At 4 NaCl wt %, the adsorption of the free methyl group gives a free energy drop of about −3 kJ/mol at $z \approx 2.2$ nm; the depth of the minimum at $z \approx 1.7$ is about −4.5 kJ/mol nm. At 10 NaCl wt % there is a free energy drop ∼−4 kJ/mol when the free methyl group is adsorbed into a hydrate cavity, and the steered methyl group is at $z \approx 2.5$ nm (see Figure 3d). The free energy minimum is about −7 kJ/mol when the pulled CH_3 group is adsorbed on the hydrate surface (see Figure 3d).

DOI: 10.1021/acscentsci.8b00076
ACS Cent. Sci. 2018, 4, 820−831

Interestingly an instantaneous hydrate-like structure is formed around the *n*-decane molecule.

The adsorption of molecule M1 on the hydrate surface is analyzed in Figure 4. The free energy profiles at 0, 4, and 10 NaCl wt % are shown in Figure 4a–c, respectively. Figure 4d is a snapshot when the headgroup atom is at $z \approx 2.6$ nm, and the surfactant tail is adsorbed on the hydrate surface; Figure 4e shows the surfactant headgroup adsorbed on the hydrate surface at $z \approx 1.9$ nm. A decrease of the free energy of adsorption of molecule M1 on the hydrate surface is observed as the salt concentration increases. At zero salt concentration, there is a free energy drop of about −2 kJ/mol when the tail is adsorbed on the hydrate surface, and the headgroup is away from the hydrate surface at $z \approx 2.6$ nm. From about $z \approx 2$ nm the free energy profile increases. At 4 NaCl wt %, the free energy profile decreases from about $z \approx 2.8$ nm when the surfactant tail is adsorbed on the hydrate surface and reaches a minimum of −4 kJ/mol at $z \approx 1.9$ nm, representing the adsorption of the surfactant head. There is no significant effect of NaCl from 0 to 4 NaCl wt %. Similarly, the free energy profile at 10 NaCl wt % shows a decrease from $z \approx 2.8$ nm (see Figure 4d) reaching a minimum of about −11 kJ/mol at $z \approx 1.9$ nm when the surfactant head is adsorbed on the hydrate surface (see Figure 4e). The surfactant is found in three main favorable positions: In one configuration the tail end is adsorbed on the hydrate surface, and the head is in the aqueous phase (see Figure 4d); in another configuration the head is adsorbed on the hydrate surface, and the tail is in the aqueous phase (not shown). In the third configuration both the tail and the head are adsorbed on the hydrate surface (see Figure 4e). The first configuration is preferred at zero salt concentration while the third configuration is the most favorable at salt concentrations of 4 and 10 NaCl wt %. We highlight the instantaneous hydrate-like structure around the head when it is adsorbed (see Figure 4e). The effect of salt in improving the efficiency of molecule M1 as hydrate antiagglomerant, in our simulations, is in line with our recent measurements.[61,62] Note that there is no alkane in the system. Molecule M1 becomes effective at higher salt concentration in full agreement with experimental observation. Surfactant M1 is the only molecule reported in the literature that has this feature.

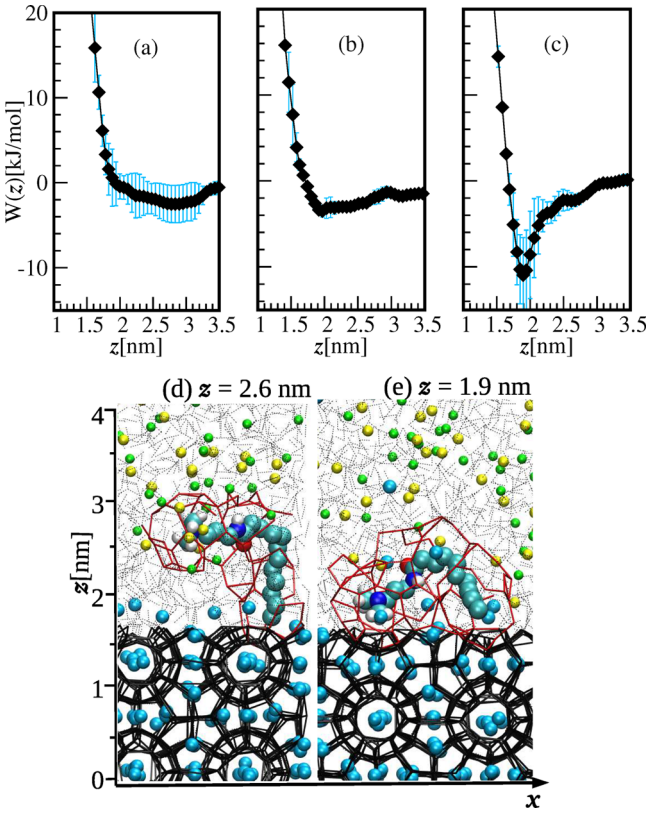

Figure 4. Adsorption of molecule M1 on the surface of methane hydrate (sI). Potential of mean force $W(z)$ as a function of the distance between the pulled headgroup atom N_a and the hydrate slab; the origin is set inside the hydrate slab. The NaCl salt concentration is (a) 0, (b) 4, and (c) 10 NaCl wt %. Snapshots showing configurations of molecule M1 at 10 NaCl wt % when the N_a headgroup atom is at (d) $z \approx 2.6$ nm and at (e) at $z \approx 1.9$ nm. The red thin lines show hydrogen bonding around molecule M1. The spring constant is k = 2000 kJ/(mol nm^2); the pulling velocity is 5×10^{-3} nm/ns, P = 300 bar, and T = 277 K.

The adsorption of molecule M2 at 0, 4, and 10 NaCl wt % is examined in Figure 5. At the three salt concentrations the adsorption of the cationic surfactant head is unfavorable. At 0 and 4 NaCl wt %, the free energy profile increases from about $z \approx 3$ nm as the surfactant headgroup approaches to the hydrate surface. At 10 NaCl wt %, there is a free energy minimum of −2.5 kJ/mol related to the adsorption of the tail on the hydrate surface when the steered headgroup atom is at $z \approx 2.7$ nm (see

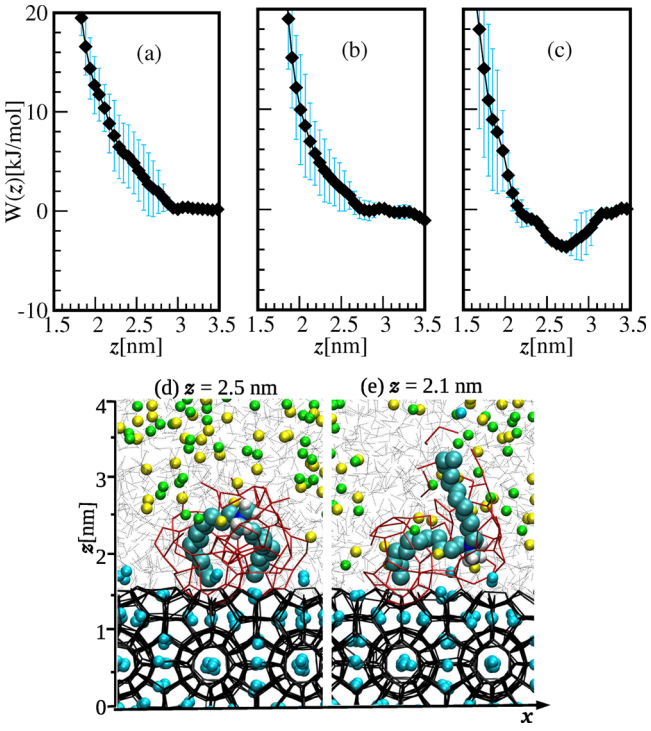

Figure 5. Adsorption of molecule M2 on the surface of methane hydrate (sI). Potential of mean force $W(z)$ as a function of the distance between the pulled headgroup atom N_c and the hydrate slab; the origin is set inside the hydrate slab. The NaCl salt concentration is (a) 0, (b) 4, and (c) 10 NaCl wt %. Snapshots showing configurations of molecule M2 at 10 NaCl wt % when the N_a headgroup atom is at (d) z = 2.5 nm, and (e) z = 2.1 nm. The red thin lines show hydrogen bonding around molecule M2. The spring constant is k = 2000 kJ/(mol nm^2); the pulling velocity is 5×10^{-3} nm/ns, P = 300 bar, and T = 277 K.

DOI: 10.1021/acscentsci.8b00076
ACS Cent. Sci. 2018, 4, 820–831

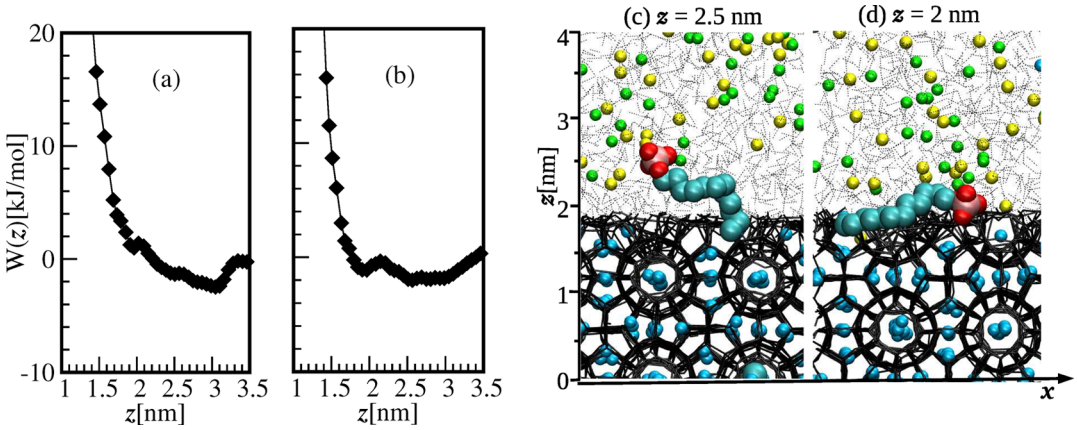

Figure 6. Adsorption of molecule M3 on the surface of methane hydrate (sI). Potential of mean force $W(z)$ as a function of the distance between the pulled headgroup atom S and the hydrate slab; the origin is set inside the hydrate slab. The NaCl salt concentration is (a) 0 and (b) 10 NaCl wt %. Snapshots showing configurations of molecule M3 at 10 NaCl wt % when the S headgroup atom is at (c) z = 2.5 nm, and (d) z = 2 nm. The spring constant is k = 2000 kJ/(mol nm^2); the pulling velocity is 5 × 10^{-3} nm/ns, P = 300 bar, and T = 277 K.

Figure 5d); from this point the free energy increases when the ionic head moves toward the hydrate surface. The free energy increase is related to the unfavorable formation of hydrate-like structures around the ionic headgroup, implying that the hydration layer around the ionic headgroup is incompatible with the hydrate structure. This is related to the difference of dielectric constant between the aqueous phase and the clathrate hydrate solid; ionic groups stay more favorably in the liquid phase due to the higher dielectric constant. In Figure 5e we see that the hydrogen bond network closes around the methane molecules of the hydrate crystal but is open around the surfactant head. The closed cavities prevent a further approach of the surfactant molecule.

The adsorption of molecule M3 on the hydrate surface is unfavorable even though tetrahedral structures may form around the SDS headgroup. The same as in surfactant M2, the free energy profile increases as the surfactant headgroup approaches to the hydrate surface at 0 and 10 NaCl wt % (see Figure 6a,b). The small free energy minimum corresponds to the adsorption of the tail on the hydrate surface when the steered headgroup atom is between 2.5 nm $\lesssim z \lesssim$ 3 nm (see Figure 6c). The minimum at $z \approx$ 2 nm corresponds to a configuration like that in Figure 6d and is related to a partial coupling between the surfactant headgroup and the hydrate structure from the tetrahedral structures (see the discussion of Figure 2q–t). The NaCl in the aqueous phase does not appreciably affect the adsorption of SDS.

The hydrate structure may significantly affect the adsorption of surfactants due to interactions of the surfactant with the guest molecules and the geometry of the cages. We conducted simulations of the adsorption of molecules M1 and M2 in the presence of structure II of propane hydrates, and we found that the adsorption of the nonionic surfactant molecule M1 on structure II is more favorable than on structure I at similar conditions; the free energy minimum by adsorption of M1 headgroup on structure sII is about −7 kJ/mol (see Figure S7a in the SI) whereas it is about −2 kJ/mol on structure sI (see Figure 4a). The adsorption of ionic headgroups on clathrate hydrates structure II is unfavorable similarly to methane hydrates (see Figure S7b in the SI).

To confirm our prediction from the potential of mean force calculations, we conducted MD simulations leaving the molecules free to allow them to look for their favorable location. We see that *n*-decane is adsorbed on the hydrate surface with one methyl group adsorbed into a cavity from the hydrate surface; the residence time is more than 40 ns in a 90 ns MD simulation (see Figure S8 in the SI). Molecule M1 is adsorbed on the hydrate surface through both the tail end and the headgroup (see Figure S9 in the SI); the residence time is more than 50 ns. In a 130 ns MD simulation molecule M2 is not adsorbed on the hydrate surface; most of the time it is excluded from the liquid layer next to the hydrate surface when it comes close to the hydrate surface (see Figure S10 in the SI). The molecular simulation results are in line with experimental data that ionic antiagglomerants are not effective where water cut is high.[31]

DISCUSSION

The preference of ionic species to stay in the aqueous phase rather than in the hydrate surface can be explained in terms of the dielectric constant difference between the two media; the dielectric constant is about 80 for the aqueous phase and about 50 for clathrate hydrates sI.[1,70] In the aqueous phase, the dipole moment of water molecules is favorably aligned by the interaction with ions. In the solid clathrate, the hydrogen bonding tends to maintain a water molecule at fixed position and orientation. Ions stay in the liquid phase because they are more favorably hydrated than in the solid clathrate where there is a strong resistance to change the water orientation due to hydrogen bonding. The ions and clathrate hydrates are incompatible. The rejection of ions from the hydrate surface and the disliking between ions and hydrocarbons are understood in similar terms. In the continuous theory of dielectrics,[71−73] a charge q near the interface between two media experiences a force from an image charge $q' = q(\epsilon_1 - \epsilon_2)/(\epsilon_2 + \epsilon_1)$; ϵ_1 and ϵ_2 are the charges of the media 1 and 2, respectively. When $\epsilon_1 > \epsilon_2$ the sign of the image charge q' is the same as the real charge q; hence, the force from the interface on q is repulsive. Our MD simulation captures the repulsive effect by the dielectric discontinuity as predicted in the classical theory of dielectrics.

The dissolution of a hydrocarbon chain in water requires a free energy cost to break hydrogen bonds and create a cavity free of water molecules.[74] Hydrophobic hydration is an indication of the disliking of *liquid* water molecules and hydrocarbon chains; the hydrocarbon interaction with a

DOI: 10.1021/acscentsci.8b00076
ACS Cent. Sci. 2018, 4, 820−831

hydrogen bond surface is more favorable than with liquid water. The segregation of hydrophobic molecules toward the hydrate surface minimizes the volume where hydrogen bonds are disrupted. Hence, hydrophobicity results in adsorption of a hydrocarbon chain at the hydrate surface.[75,76] The favorable adsorption of hydrophobic groups on the hydrates surface has been indicated in molecular simulation studies.[41] Pure hydrocarbon chains may not be classified as hydrate inhibitors because their solubility in aqueous phase is extremely low. In hydrate antiagglomeration the oil phase serves as the medium where antiagglomeration takes place. Our results for *n*-decane indicate that hydrocarbons may have an active role in hydrate antiagglomeration. This suggestion is in line with recent experimental results.[61,62]

The primary role of the headgroup is to aid dissolution of the surfactant in aqueous solution. In solution the surfactants may be adsorbed on the hydrates surface. Based on the potential of mean force the nonionic surfactant M1 is favorably adsorbed on the hydrate surface by the tail and the head. In rocking cell experiments molecule M1 has been demonstrated to be an effective antiagglomerant[31,63,64] in the absence of liquid hydrocarbons.[64] The surfactant M2 may be an effective hydrate antiagglomerant when there is a liquid hydrocarbon phase;[64] it is not effective when there are no substantial amounts of hydrocarbons in the system. Quaternary ammonium surfactants (QASs) have been developed and patented as antiagglomerants and are effective in the presence of liquid hydrocarbons.[30] The structure of QAS consists of a central ammonium group bonded to four *n*-alkyl chains that may be of different lengths. Our results suggest that the QAS can be attached to the hydrate surface through the hydrocarbon chains but unlikely by direct adsorption of the ionic headgroup. Effective antiagglomerant QASs consist of two or more *n*-butyl chains[25,30] that may attach to the hydrate surface. The ions in the aqueous phase create more hydrophobic repulsion of the hydrocarbon chains in the solution toward the hydrate surface. In experiments, the performance of hydrate antiagglomerants is improved with NaCl[30,61,62] as mentioned above.

CONCLUSIONS

The main conclusions from this work are as follows:

- Hydrophobic molecules induce instantaneous structuring of water molecules in the bulk aqueous phase similar to clathrate hydrates which is referred to as hydrophobic hydration. We quantify hydrophobic hydration of methane, *n*-decane, and a nonionic and an ionic surfactant by the number of hydrogen bonds and tetrahedrality of water molecules.
- Hydrophobic hydration is enhanced at the end of hydrocarbon chains and around the nonionic amide surfactant headgroup. Hydrophobic hydration is reduced at the middle of hydrocarbon chains and by NaCl ions.
- The structure of water around the ionic headgroups is different from hydrophobic hydration. A significant reduction of hydrogen bonds and tetrahedral structures is observed around the cationic ammonium headgroup. On the contrary, the anionic headgroup of the sodium dodecyl surfactant promotes the formation of tetrahedral water structures which may be related to the increase of the hydrate nucleation rate.
- Hydrophobic hydration is directly related to the affinity of the chemical groups for the surface of hydrates; the hydrocarbon chain end and the nonionic amide group are preferentially adsorbed on the hydrate surface while adsorption of ions and the ammonium group is unfavorable. Hydrophobic groups are hydrophobically hydrated on the hydrate surface.
- The underlying cause for ionic groups to be repelled from hydrophobic molecules and from the hydrate surface toward the liquid phase is due to the difference of dielectric constants. Ionic groups are more favorably hydrated in the aqueous phase, and they are not part of the clathrate hydrate solid.
- The adsorption of a solute molecule on the hydrate surface is enhanced by NaCl ions in the aqueous phase. The affinity of ions for water molecules and the dislike for hydrophobic groups drive the surfactant molecules to the hydrate−water interface.
- The adsorption of nonionic groups on clathrate hydrates is more favorable on structure II than on structure I. The adsorption of ionic surfactants is unfavorable in both structures.

MODELS AND METHODS

We represent hydrocarbon chains like *n*-decane and the surfactants' tail using the TraPPE united atom model of liquid hydrocarbons.[77] Molecule M1 is cocamidopropyl dimethylamine, a nonionic surfactant which consists of a dimethyl amine in the head, an amide in the middle, and a hydrocarbon tail. We take into account the full atomic structure of the amine and amide groups using the OPLS-AA force field.[78,79] Molecule M2, didodecyl dimethylammonium chloride, is a quaternary ammonium surfactant, containing an ammonium headgroup bonded to two methyl and two dodecyl groups. The full atomic structure of the ammonium headgroup is taken into account using the OPLS-AA force field.[80] The partial charges and Lennard-Jones parameters of molecules M1, M2, and M3 are provided in Tables S1−S3 in the SI, respectively.

Water molecules are simulated using the TIP4P-ice model which describes accurately the three-phase equilibrium of methane hydrates.[81,82] Methane molecules are described as spherical particles interacting via a Lennard-Jones potential; the parameters are σ = 0.373 nm and ϵ = 1.23 kJ/mol.[83] The interaction between dissimilar atoms is computed using the Lorentz−Berthelot combining rules. We verified the validity of the force field parameters and combination rules by computing the free energy of solution of the trimethylamine molecule $[N(CH_3)_3]$ and the enthalpy of hydration of the tetramethylammonium ion $[N(CH_3)_4^+]$. Both values are in agreement with experimental measurements (see the SI).

To simulate the adsorption of solutes on the hydrate surface we employ the setup shown in Figure 1b consisting of a hydrate slab next to an aqueous solution. The hydrate slab is made of 4 × 4 × 3 unit cells of methane hydrate crystal (2204 water molecules and 384 methane molecules). The focus of our work is on structure I (sI) of clathrate hydrates, and some additional studies are performed on structure II (sII). Unless it is explicitly stated the hydrate structure is sI. The aqueous phase is made of 5700 water molecules and contains 20 methane molecules; 72 and 180 ionic NaCl pairs are added in the aqueous phase at 4 and 10 NaCl wt %, respectively. The hydrate slab dimensions are 4.8 nm × 4.8 nm × 3.6 nm along

DOI: 10.1021/acscentsci.8b00076
ACS Cent. Sci. 2018, 4, 820−831

x, y, and z, respectively. The simulation box dimensions are 4.8 nm × 4.8 nm along the x and y directions, respectively, and the box length along the z direction is around 12.2 nm. Adsorption on structure II of clathrate hydrates is simulated for methane and molecules M1 and M2. Adsorption of methane is simulated to validate the steered molecular dynamics method using a setup similar to that employed by Yagasaki et al.[45] of methane hydrates sII; the stable phase of methane hydrates is sI. The hydrate slab for methane adsorption consists of 2 × 2 × 2 sII unit cells and is made of 1088 water molecules and 192 methane molecules; the aqueous phase is made of 2162 water molecules. The adsorption of molecules M1 and M2 on clathrate hydrate sII is simulated using a hydrate slab consisting of 3 × 3 × 2 unit cells and constituted by 2448 water molecules and 144 propane molecules; sII is the stable phase of propane hydrates. The aqueous phase is made of 6688 water molecules. The study of the solute molecules in the bulk aqueous phase is performed without the hydrate slab.

Steered Molecular Dynamics Simulations. We employ steered molecular dynamics to investigate the adsorption of solute molecules on the hydrate surface. The technique consists of connecting a dummy atom to target atom of the solute molecule and then moving the dummy atom at constant velocity v; the connection is through a harmonic potential with a spring constant k. The force exerted by the molecules in the medium is the negative of the pulling force. The mean force $\overline{F}_z$ is the average force over 20 ns of pulling. The work to transfer the molecule between two points is given by

$$W(z) = -\int_{z_0}^{z} \overline{F}_z(z')\, dz' \tag{1}$$

$W(z)$ is the potential of mean force as a function of the distance to the hydrate slab z; z_0 is a reference position of the atom in the solute molecule hooked to the dummy atom. At constant pressure and temperature the work is the Gibbs free energy change by moving the molecule, $W = \Delta G$.

In statistical mechanics of homogeneous fluids the potential of mean force between two particles $W(\mathbf{r})$ is related to the pair correlation function $g^{(2)}(\mathbf{r})$ by[84,85]

$$g^{(2)}(\mathbf{r}) = \exp\{-\beta W(\mathbf{r})\} \tag{2}$$

where $\beta = 1/(k_B T)$; k_B is the Boltzmann constant, and T the absolute temperature. In theory of statistical mechanics of inhomogeneous fluids $W(z)$ is related to the density profile $\rho(z)$ by[86]

$$\rho(z) = \rho_b \exp\{-\beta W(z)\} \tag{3}$$

where ρ_b is the reference density (bulk) of an inhomogeneous fluid.

Steered molecular dynamics (SMD) simulations are performed in the following way: (1) A 0.5 ns run is carried out to equilibrate the system at the prescribed pressure and temperature; in this step we use the Berendsen[87] thermostat (τ_T = 0.1 ps) and barostat (τ_P = 0.5 ps). The molecule is initially placed about 3 nm away from the hydrate surface. (2) Steered molecular dynamics simulations are performed by pulling one atom of the solute molecule along the z direction. For n-decane the pulling is applied on one methyl group (end group); for molecules M1, M2, and M3 the pulling is applied on the N_a, N_c, and S headgroup atoms, respectively. Other atoms are not steered or constrained, and steering is not applied in the x and y directions. We use a spring constant of k = 2000 kJ/(mol nm^2), and the pulling is performed at a velocity of $v_z = 5 \times 10^{-3}$ nm/ns along the z direction. Steered molecular dynamics gives similar results of the potential of mean force as the umbrella sampling method (see Figures S11 and S12 in the SI). The simulation time is about 600 ns per run, and the CPU time is about 160 ns/day using four P-100 GPU cards from Nvidia. The force running average $\overline{F}_z(z)$ is calculated over intervals of 20 ns; within this time frame the molecule explores a large number of orientations and positions in the x and y directions (see Figure S13 in the SI). Each plot of the potential of mean force and the error bars are calculated from at least three independent simulation runs. The temperature and pressure are controlled using the Nosé–Hoover[88,89] thermostat (τ_T = 2 ps) and the Parrinello–Rahman barostat (τ_P = 4 ps), respectively. Simulations are performed at T = 277 K and P = 300 bar. A time-step of 2 fs is used to integrate Newton's equation of motion. Short-range interactions are truncated at 1.2 nm, and long-range electrostatic interactions are computed using the smooth particle mesh Ewald summation. Three-dimensional-periodic boundary conditions are applied. The simulations are performed using the open source code Gromacs.[90−92]

■ ASSOCIATED CONTENT

Supporting Information

The Supporting Information is available free of charge on the ACS Publications website at DOI: 10.1021/acscentsci.8b00076.

Tables including the force field parameters; verification of steered molecular dynamics simulation; validation of force field parameters of surfactant headgroups; analysis of the orientation of the solute molecule in steered molecular dynamics; effect of NaCl Salt in the hydrates three-phase equilibrium; and additional simulation data of solutes in the bulk (PDF)

■ AUTHOR INFORMATION

Corresponding Author

*E-mail: abbas.firoozabadi@yale.edu. Phone: +1 (650) 326-9172. Fax: +1 (650) 472-9285.

ORCID

Abbas Firoozabadi: 0000-0001-6102-9534

Notes

The authors declare no competing financial interest.

Safety statement: no unexpected or unusually high safety hazards were encountered.

■ ACKNOWLEDGMENTS

We thank the member companies of the Reservoir Engineering Research Institute (RERI) for their financial support of this work.

■ REFERENCES

(1) Sloan, E. D.; Koh, C. A. *Clathrate Hydrates of Natural Gases*; CRC Press: Boca Raton, FL, 2008.

(2) Buffett, B. A. Clathrate Hydrates. *Annu. Rev. Earth Planet. Sci.* **2000**, *28*, 477−507.

(3) Walsh, M. R.; Koh, C. A.; Sloan, E. D.; Sum, A. K.; Wu, D. T. Microsecond Simulations of Spontaneous Methane Hydrate Nucleation and Growth. *Science* **2009**, *326*, 1095−1098.

(4) Walsh, M. R.; Rainey, J. D.; Lafond, P. G.; Park, D.-H.; Beckham, G. T.; Jones, M. D.; Lee, K.-H.; Koh, C. A.; Sloan, E. D.; Wu, D. T.;

DOI: 10.1021/acscentsci.8b00076
ACS Cent. Sci. 2018, 4, 820−831

Sum, A. K. The Cages, Dynamics, and Structuring of Incipient Methane Clathrate Hydrates. *Phys. Chem. Chem. Phys.* **2011**, *13*, 19951−19959.
(5) Walsh, M. R.; Beckham, G. T.; Koh, C. A.; Sloan, E. D.; Wu, D. T.; Sum, A. K. Methane Hydrate Nucleation Rates from Molecular Dynamics Simulations: Effects of Aqueous Methane Concentration, Interfacial Curvature, and System Size. *J. Phys. Chem. C* **2011**, *115*, 21241−21248.
(6) Jacobson, L. C.; Hujo, W.; Molinero, V. Thermodynamic Stability and Growth of Guest-Free Clathrate Hydrates. *J. Phys. Chem. B* **2009**, *113*, 10298−10307.
(7) Jacobson, L. C.; Hujo, W.; Molinero, V. Amorphous Precursors in the Nucleation of Clathrate Hydrates. *J. Am. Chem. Soc.* **2010**, *132*, 11806−11811.
(8) Liang, S.; Kusalik, P. G. Exploring Nucleation of H_2S Hydrates. *Chem. Sci.* **2011**, *2*, 1286−1292.
(9) Ripmeester, J. A.; Alavi, S. Molecular Simulations of Methane Hydrate Nucleation. *ChemPhysChem* **2010**, *11*, 978−980.
(10) Guo, G.-J.; Zhang, Y.-G.; Liu, H. Effect of Methane Adsorption on the Lifetime of a Dodecahedral. *J. Phys. Chem. C* **2007**, *111*, 2595−2606.
(11) Guo, G.-J.; Rodger, P. M. Solubility of Aqueous Methane Under Metastable Conditions. *J. Phys. Chem. B* **2013**, *117*, 6498−6504.
(12) Sarupria, S.; Debenedetti, P. G. Homogeneous Nucleation of Methane Hydrate in Microsecond Molecular Dynamics Simulations. *J. Phys. Chem. Lett.* **2012**, *3*, 2942−2947.
(13) Jiménez-Ángeles, F.; Firoozabadi, A. Nucleation of Methane Hydrates at Moderate Subcooling by Molecular Dynamics Simulations. *J. Phys. Chem. C* **2014**, *118*, 11310−11318.
(14) Jiménez-Ángeles, F.; Firoozabadi, A. Enhanced Hydrate Nucleation near the Limit of Stability. *J. Phys. Chem. C* **2015**, *119*, 8798−8804.
(15) Zhang, J. S.; Lee, S.; Lee, J. W. Kinetics of Methane Hydrate Formation from SDS Solution. *Ind. Eng. Chem. Res.* **2007**, *46*, 6353−6359.
(16) Kang, H.; Ahn, Y.-H.; Koh, D.-Y.; Baek, S.; Lee, J. W.; Lee, H. Rapid Clathrate Hydrate Formation Using a Heavy Guest Molecule with Sodium Dodecyl Sulfate. *Ind. Eng. Chem. Res.* **2016**, *55*, 6079−6084.
(17) Zhong, Y.; Rogers, R. Surfactant Effects on Gas Hydrate Formation. *Chem. Eng. Sci.* **2000**, *55*, 4175−4187.
(18) Karaaslan, U.; Parlaktuna, M. Surfactants as Hydrate Promoters? *Energy Fuels* **2000**, *14*, 1103−1107.
(19) Lo, C.; Zhang, J. S.; Somasundaran, P.; Lu, S.; Couzis, A.; Lee, J. W. Adsorption of Surfactants on Two Different Hydrates. *Langmuir* **2008**, *24*, 12723−12726.
(20) Salako, O.; Lo, C.; Zhang, J.; Couzis, A.; Somasundaran, P.; Lee, J. Adsorption of Sodium Dodecyl Sulfate onto Clathrate Hydrates in the Presence of Salt. *J. Colloid Interface Sci.* **2012**, *386*, 333−337.
(21) Salako, O.; Lo, C.; Couzis, A.; Somasundaran, P.; Lee, J. Adsorption of Gemini surfactants onto clathrate hydrates. *J. Colloid Interface Sci.* **2013**, *412*, 1−6.
(22) Jiménez-Ángeles, F.; Khoshnood, A.; Firoozabadi, A. Molecular Dynamics Simulation of the Adsorption and Aggregation of Ionic Surfactants at Liquid−Solid Interfaces. *J. Phys. Chem. C* **2017**, *121*, 25908−25920.
(23) Ruiz-Morales, Y.; Romero-Martínez, A. Coarse-Grain Molecular Dynamics Simulations To Investigate the Bulk Viscosity and Critical Micelle Concentration of the Ionic Surfactant Sodium Dodecyl Sulfate (SDS) in Aqueous Solution. *J. Phys. Chem. B* **2018**, *122*, 3931−3943.
(24) Koh, C.; Westacott, R.; Zhang, W.; Hirachand, K.; Creek, J.; Soper, A. Mechanisms of Gas Hydrate Formation and Inhibition. *Fluid Phase Equilib.* **2002**, *194−197*, 143−151.
(25) Kelland, M. A. History of the Development of Low Dosage Hydrate Inhibitors. *Energy Fuels* **2006**, *20*, 825−847.
(26) Tung, Y.-T.; Chen, L.-J.; Chen, Y.-P.; Lin, S.-T. Molecular Dynamics Study on the Growth of Structure I Methane Hydrate in Aqueous Solution of Sodium Chloride. *J. Phys. Chem. B* **2012**, *116*, 14115−14125.
(27) Jager, M.; Sloan, E. The Effect of Pressure on Methane Hydration in Pure Water and Sodium Chloride Solutions. *Fluid Phase Equilib.* **2001**, *185*, 89−99.
(28) Perrin, A.; Musa, O. M.; Steed, J. W. The Chemistry of Low Dosage Clathrate Hydrate Inhibitors. *Chem. Soc. Rev.* **2013**, *42*, 1996−2015.
(29) Anderson, B. J.; Tester, J. W.; Borghi, G. P.; Trout, B. L. Properties of Inhibitors of Methane Hydrate Formation via Molecular Dynamics Simulations. *J. Am. Chem. Soc.* **2005**, *127*, 17852−17862.
(30) Chua, P. C.; Kelland, M. A. Study of the Gas Hydrate Anti-agglomerant Performance of a Series of *n*-Alkyl-tri(*n*-butyl)-ammonium Bromides. *Energy Fuels* **2013**, *27*, 1285−1292.
(31) Sun, M.; Firoozabadi, A. New Surfactant for Hydrate Anti-Agglomeration in Hydrocarbon Flowlines and Seabed Oil Capture. *J. Colloid Interface Sci.* **2013**, *402*, 312−319.
(32) Walker, V. K.; Zeng, H.; Ohno, H.; Daraboina, N.; Sharifi, H.; Bagherzadeh, S. A.; Alavi, S.; Englezos, P. Antifreeze Proteins as Gas Hydrate Inhibitors. *Can. J. Chem.* **2015**, *93*, 839−849.
(33) Sun, T.; Davies, P. L.; Walker, V. K. Structural Basis for the Inhibition of Gas Hydrates by -Helical Antifreeze Proteins. *Biophys. J.* **2015**, *109*, 1698−1705.
(34) Alireza Bagherzadeh, S.; Alavi, S.; Ripmeester, J. A.; Englezos, P. Why Ice-binding Type I Antifreeze Protein Acts as a Gas Hydrate Crystal Inhibitor. *Phys. Chem. Chem. Phys.* **2015**, *17*, 9984−9990.
(35) Sa, J.-H.; Kwak, G.-H.; Han, K.; Ahn, D.; Cho, S. J.; Lee, J. D.; Lee, K.-H. Inhibition of Methane and Natural Gas Hydrate Formation by Altering the Structure of Water with Amino Acids. *Sci. Rep.* **2016**, *6*, 31582.
(36) Perfeldt, C. M.; Chua, P. C.; Daraboina, N.; Friis, D.; Kristiansen, E.; Ramlv, H.; Woodley, J. M.; Kelland, M. A.; von Solms, N. Inhibition of Gas Hydrate Nucleation and Growth: Efficacy of an Antifreeze Protein from the Longhorn Beetle Rhagium mordax. *Energy Fuels* **2014**, *28*, 3666−3672.
(37) Larsen, R.; Knight, C. A.; Sloan, E. D. Clathrate Hydrate Growth and Inhibition. *Fluid Phase Equilib.* **1998**, *150−151*, 353−360.
(38) King, H. E.; Hutter, J. L.; Lin, M. Y.; Sun, T. Polymer Conformations of Gas-Hydrate Kinetic Inhibitors: A Small-Angle Neutron Scattering Study. *J. Chem. Phys.* **2000**, *112*, 2523−2532.
(39) Carver, T. J.; Drew, M. G. B.; Rodger, P. M. Characterisation of the 111 Growth Planes of a Type II Gas Hydrate and Study of the Mechanism of Kinetic Inhibition by Poly(Vinylpyrrolidone). *J. Chem. Soc., Faraday Trans.* **1996**, *92*, 5029−5033.
(40) Carver, T. J.; Drew, M. G.; Rodger, P. M. Configuration-Biased Monte Carlo Simulations of Poly(Vinylpyrrolidone) at a Gas Hydrate Crystal Surface. *Ann. N. Y. Acad. Sci.* **2000**, *912*, 658−668.
(41) Storr, M. T.; Taylor, P. C.; Monfort, J.-P.; Rodger, P. M. Kinetic Inhibitor of Hydrate Crystallization. *J. Am. Chem. Soc.* **2004**, *126*, 1569−1576.
(42) Duffy, D. M.; Moon, C.; Rodger, P. M. Computer-Assisted Design of Oil Additives: Hydrate and Wax Inhibitors. *Mol. Phys.* **2004**, *102*, 203−210.
(43) Gómez Gualdrón, D. A.; Balbuena, P. B. Classical Molecular Dynamics of Clathrate-Methane-Water-Kinetic Inhibitor Composite Systems. *J. Phys. Chem. C* **2007**, *111*, 15554−15564.
(44) Moon, C.; Hawtin, R. W.; Rodger, P. M. Nucleation and Control of Clathrate Hydrates: Insights From Simulation. *Faraday Discuss.* **2007**, *136*, 367−382 discussion 395−407.
(45) Yagasaki, T.; Matsumoto, M.; Tanaka, H. Adsorption Mechanism of Inhibitor and Guest Molecules on the Surface of Gas Hydrates. *J. Am. Chem. Soc.* **2015**, *137*, 12079−12085.
(46) Phan, A.; Bui, T.; Acosta, E.; Krishnamurthy, P.; Striolo, A. Molecular Mechanisms Responsible for Hydrate Anti-Agglomerant Performance. *Phys. Chem. Chem. Phys.* **2016**, *18*, 24859−24871.

DOI: 10.1021/acscentsci.8b00076
ACS Cent. Sci. 2018, 4, 820−831

(47) Bui, T.; Phan, A.; Monteiro, D.; Lan, Q.; Ceglio, M.; Acosta, E.; Krishnamurthy, P.; Striolo, A. Evidence of Structure-Performance Relation for Surfactants Used as Antiagglomerants for Hydrate Management. *Langmuir* **2017**, *33*, 2263−2274.
(48) Bellucci, M. A.; Walsh, M. R.; Trout, B. L. Molecular Dynamics Analysis of Anti-Agglomerant Surface Adsorption in Natural Gas Hydrates. *J. Phys. Chem. C* **2018**, *122*, 2673−2683.
(49) Galamba, N. Water Tetrahedrons, Hydrogen-Bond Dynamics, and the Orientational Mobility of Water around Hydrophobic Solutes. *J. Phys. Chem. B* **2014**, *118*, 4169−4176.
(50) Galamba, N. Waters Structure around Hydrophobic Solutes and the Iceberg Model. *J. Phys. Chem. B* **2013**, *117*, 2153−2159.
(51) Davis, J. G.; Gierszal, K. P.; Wang, P.; Ben-Amotz, D. Water Structural Transformation at Molecular Hydrophobic Interfaces. *Nature* **2012**, *491*, 582−585.
(52) Davis, J. G.; Rankin, B. M.; Gierszal, K. P.; Ben-Amotz, D. On the Cooperative Formation of Non-Hydrogen-Bonded Water at Molecular Hydrophobic Interfaces. *Nat. Chem.* **2013**, *5*, 796−802.
(53) Perera, P. N.; Fega, K. R.; Lawrence, C.; Sundstrom, E. J.; Tomlinson-Phillips, J.; Ben-Amotz, D. Observation of Water Dangling OH Bonds around Dissolved Nonpolar Groups. *Proc. Natl. Acad. Sci. U. S. A.* **2009**, *106*, 12230−12234.
(54) Raschke, T. M.; Levitt, M. Nonpolar Solutes Enhance Water Structure Within hydration Shells While Reducing Interactions Between Them. *Proc. Natl. Acad. Sci. U. S. A.* **2005**, *102*, 6777−6782.
(55) Kim, J.; Tian, Y.; Wu, J. Thermodynamic and Structural Evidence for Reduced Hydrogen Bonding among Water Molecules near Small Hydrophobic Solutes. *J. Phys. Chem. B* **2015**, *119*, 12108−12116.
(56) Grdadolnik, J.; Merzel, F.; Avbelj, F. Origin of Hydrophobicity and Enhanced Water Hydrogen Bond Strength Near Purely Hydrophobic Solutes. *Proc. Natl. Acad. Sci. U. S. A.* **2017**, *114*, 322−327.
(57) Frank, H. S.; Evans, M. W. Free Volume and Entropy in Condensed Systems III. Entropy in Binary Liquid Mixtures; Partial Molal Entropy in Dilute Solutions; Structure and Thermodynamics in Aqueous Electrolytes. *J. Chem. Phys.* **1945**, *13*, 507−532.
(58) Patel, A. J.; Varilly, P.; Jamadagni, S. N.; Hagan, M. F.; Chandler, D.; Garde, S. Sitting at the Edge: How Biomolecules use Hydrophobicity to Tune Their Interactions and Function. *J. Phys. Chem. B* **2012**, *116*, 2498−2503.
(59) Meister, K.; Strazdaite, S.; DeVries, A. L.; Lotze, S.; Olijve, L. L. C.; Voets, I. K.; Bakker, H. J. Observation of Ice-Like Water Layers at an Aqueous Protein Surface. *Proc. Natl. Acad. Sci. U. S. A.* **2014**, *111*, 17732−17736.
(60) Laage, D.; Elsaesser, T.; Hynes, J. T. Water Dynamics in the Hydration Shells of Biomolecules. *Chem. Rev.* **2017**, *117*, 10694−10725.
(61) Dong, S.; Li, M.; Firoozabadi, A. Effect of Salt and Water Cuts on Hydrate Anti-Agglomeration in a Gas Condensate System at High Pressure. *Fuel* **2017**, *210*, 713−720.
(62) Dong, S.; Firoozabadi, A. Hydrate Anti-Agglomeration and Synergy Effect in Normal Octane at Varying Water Cuts and Salt Concentrations. *J. Chem. Thermodyn.* **2017**, *117*, 214−222.
(63) Sun, M.; Firoozabadi, A. Natural Gas Hydrate Particles in Oil-Free Systems with Kinetic Inhibition and Slurry Viscosity Reduction. *Energy Fuels* **2014**, *28*, 1890−1895.
(64) Sun, M.; Firoozabadi, A. Gas Hydrate Powder Formation − Ultimate Solution in Natural Gas Flow Assurance. *Fuel* **2015**, *146*, 1−5.
(65) Athawale, M. V.; Sarupria, S.; Garde, S. Enthalpy-Entropy Contributions to Salt and Osmolyte Effects on Molecular-Scale Hydrophobic Hydration and Interactions. *J. Phys. Chem. B* **2008**, *112*, 5661−5670.
(66) Holzmann, J.; Ludwig, R.; Geiger, A.; Paschek, D. Temperature and Concentration Effects on the Solvophobic Solvation of Methane in Aqueous Salt Solutions. *ChemPhysChem* **2008**, *9*, 2722−2730.
(67) Bernal, J. D.; Fowler, R. H. A Theory of Water and Ionic Solution, with Particular Reference to Hydrogen and Hydroxyl Ions. *J. Chem. Phys.* **1933**, *1*, 515−548.
(68) Baez, L.; Clancy, P. Computer Simulation of the Crystal Growth and Dissolution of Natural Gas Hydrates. *Ann. N. Y. Acad. Sci.* **1994**, *715*, 177−186.
(69) Ghosh, T.; Kalra, A.; Garde, S. On the Salt-Induced Stabilization of Pair and Many-body Hydrophobic Interactions. *J. Phys. Chem. B* **2005**, *109*, 642−651.
(70) Gough, S. R.; Whalley, E.; Davidson, D. W. Dielectric Properties of the Hydrates of Argon and Nitrogen. *Can. J. Chem.* **1968**, *46*, 1673−1681.
(71) Jackson, J. D. *Classical Electrodynamics*, 3rd ed.; John Wiley & Sons, Inc.: Singapore, 1998.
(72) Zwanikken, J. W.; Olvera de la Cruz, M. Tunable Soft Structure in Charged Fluids Confined by Dielectric Interfaces. *Proc. Natl. Acad. Sci. U. S. A.* **2013**, *110*, 5301−5308.
(73) Messina, R. Image Charges in Spherical Geometry: Application to Colloidal Systems. *J. Chem. Phys.* **2002**, *117*, 11062−11074.
(74) Chandler, D. Interfaces and the Driving Force of Hydrophobic Assembly. *Nature* **2005**, *437*, 640−647.
(75) Ball, P. Water as an Active Constituent in Cell Biology. *Chem. Rev.* **2008**, *108*, 74−108.
(76) Chandler, D. Physical Chemistry: Oil on Troubled Waters. *Nature* **2007**, *445*, 831−832.
(77) Martin, M. G.; Siepmann, J. I. Transferable Potentials for Phase Equilibria. 1. United-Atom Description of n-Alkanes. *J. Phys. Chem. B* **1998**, *102*, 2569−2577.
(78) Rizzo, R. C.; Jorgensen, W. L. OPLS All-Atom Model for Amines: Resolution of the Amine Hydration Problem. *J. Am. Chem. Soc.* **1999**, *121*, 4827−4836.
(79) Jorgensen, W. L.; Maxwell, D. S.; Tirado-Rives, J. Development and Testing of the OPLS All-Atom Force Field on Conformational Energetics and Properties of Organic Liquids. *J. Am. Chem. Soc.* **1996**, *118*, 11225−11236.
(80) Jorgensen, W. L.; Gao, J. Monte Carlo Simulations of the Hydration of Ammonium and Carboxylate Ions. *J. Phys. Chem.* **1986**, *90*, 2174−2182.
(81) Abascal, J. L. F.; Sanz, E.; García Fernández, R.; Vega, C. A. Potential Model for the Study of Ices and Amorphous Water: TIP4P/Ice. *J. Chem. Phys.* **2005**, *122*, 234511-1−234511-9.
(82) Conde, M. R.; Vega, C. Determining the Three-Phase Coexistence Line in Methane Hydrates Using Computer Simulations. *J. Chem. Phys.* **2010**, *133*, 064507-1−064507-12.
(83) Calero, S.; Dubbeldam, D.; Krishna, R.; Smit, B.; Vlugt, T. J. H.; Denayer, J. F. M.; Martens, J.; Maesen, T. L. M. Understanding the Role of Sodium During Adsorption: A Force Field for Alkanes in Sodium-Exchanged Faujasites. *J. Am. Chem. Soc.* **2004**, *126*, 11377−11386.
(84) McQuarrie, D. A. *Statistical Mechanics*; Harper & Row: New York, 1976.
(85) Kirkwood, J. G. Statistical Mechanics of Fluid Mixtures. *J. Chem. Phys.* **1935**, *3*, 300−313.
(86) Henderson, D., Ed. *Fundamentals of Inhomogeneous Fluids*; Marcel Dekker, Inc: New York, 1992.
(87) Berendsen, H. J. C.; Postma, J. P. M.; van Gunsteren, W. F.; Di Nola, A.; Haak, J. R. Molecular-Dynamics with Coupling to an External Bath. *J. Chem. Phys.* **1984**, *81*, 3684−3690.
(88) Nosé, S. A. Unified Formulation of the Constant Temperature Molecular-Dynamics Methods. *J. Chem. Phys.* **1984**, *81*, 511−519.
(89) Hoover, W. G. Canonical dynamics: Equilibrium Phase-Space Distributions. *Phys. Rev. A: At., Mol., Opt. Phys.* **1985**, *31*, 1695−1697.
(90) Berendsen, H.; Spoel, D. V. D.; Drunen, R. V. Gromacs: A Message-Passing Parallel Molecular Dynamics Implementation. *Comput. Phys. Commun.* **1995**, *91*, 43−56.
(91) Van Der Spoel, D.; Lindahl, E.; Hess, B.; Groenhof, G.; Mark, A. E.; Berendsen, H. J. C. GROMACS: Fast, Flexible, and Free. *J. Comput. Chem.* **2005**, *26*, 1701−1718.

DOI: 10.1021/acscentsci.8b00076
ACS Cent. Sci. 2018, 4, 820−831

(92) Hess, B.; Kuttner, C.; van der Spoel, D.; Lindahl, E. GROMACS 4: Algorithms for Highly Efficient, Load-Balanced, and Scalable Molecular Simulation. *J. Chem. Theory Comput.* **2008**, *4*, 435−447.

DOI: 10.1021/acscentsci.8b00076
ACS Cent. Sci. 2018, 4, 820−831